THE JOURNAL OF BIOLOGICAL CHEMISTRY VOL. 281, NO. 49, pp. 37803–37812, December 8, 2006

Structural Determinants in the Group III Truncated Hemoglobin from *Campylobacter jejuni*

Received for publication, July 31, 2006, and in revised form, September 26, 2006 Published, JBC Papers in Press, October 5, 2006, DOI 10.1074/jbc.M607254200

Marco Nardini[‡], Alessandra Pesce[§], Marie Labarre[¶], Christian Richard[¶], Alessandro Bolli[‖], Paolo Ascenzi[‖], Michel Guertin[¶], and Martino Bolognesi[‡1]**

*From the [‡]Department of Biomolecular Sciences and Biotechnology, and CNR-INFM, University of Milano, I-20131 Milano, Italy, the [§]Department of Physics, CNR-INFM and Center for Excellence in Biomedical Research, University of Genova, I-16146 Genova, Italy, the [¶]Departement de Biochimie et de Microbiologie, Pavillon Marchand, Université Laval, Faculté des Sciences et de Génie, Quebec G1K 7P4, Canada, the [‖]Department of Biology and Interdepartmental Laboratory for Electron Microscopy, University "Roma Tre," Roma I-00146, and the **National Institute for Infectious Diseases I.R.C.C.S."Lazzaro Spallanzani," Roma I-00149, Italy*

Truncated hemoglobins (trHbs) constitute a distinct lineage in the globin superfamily, distantly related in size and fold to myoglobin and monomeric hemoglobins. Their phylogenetic analyses revealed that three groups (I, II, and III) compose the trHb family. Group I and II trHbs adopt a simplified globin fold, essentially composed of a 2-on-2 α-helical sandwich, wrapped around the heme group. So far no structural data have been reported for group III trHbs. Here we report the three-dimensional structure of the group III trHbP from the eubacterium *Campylobacter jejuni*. The 2.15-Å resolution crystal structure of *C. jejuni* trHbP (cyano-met form) shows that the 2-on-2 trHb fold is substantially conserved in the trHb group III, despite the absence of the Gly-based sequence motifs that were considered necessary for the attainment of the trHb specific fold. The heme crevice presents important structural modifications in the C-E region and in the FG helical hinge, with novel surface clefts at the proximal heme site. Contrary to what has been observed for group I and II trHbs, no protein matrix tunnel/cavity system is evident in *C. jejuni* trHbP. A gating movement of His(E7) side chain (found in two alternate conformations in the crystal structure) may be instrumental for ligand entry to the heme distal site. Sequence conservation allows extrapolating part of the structural results here reported to the whole trHb group III.

Recent phylogeny of the globin superfamily indicates that it contains three lineages belonging to two structural classes: one showing a 3-on-3 α-helical sandwich (animal, plant, and chimeric globins) and one having a 2-on-2 α-helical sandwich (truncated hemoglobins: trHbs).[2] Although no definitive conclusion can be drawn about the ancestral state of the globin fold, the occurrence of the 2-on-2-fold, but not of an isolated 3-on-3 fold, in all three kingdoms of life suggests that the 2-on-2 fold is the ancestral fold. On the other hand, functional studies indicate that the predominant function of globins would be enzymatic, O_2 transport and storage being a specialized function associated with the evolution of metazoans (1).

TrHbs are widely distributed in eubacteria and plants and are found in some unicellular eukaryotes. They are distantly related to the 3-on-3 globins, showing less than 20% overall identity with the latter (2). Phylogenetic analysis based on protein sequences shows that trHbs branch into three groups, designated I, II, and III (2, 3), whose members are distinguished by the N, O, and P suffixes, respectively. Group I and group II trHbs further separate into two and four subgroups, respectively, whereas group III trHbs display a high level of overall conservation. Sequence identity between trHbs from different groups is low (≤20% overall identity), but may be higher than 80% within a given group. TrHbs are largely present in eubacteria, with some bacteria displaying more than one trHb belonging to different groups. Analysis of the distribution of trHbs suggested a scenario for the evolution of the different groups where the group II trHb gene is the ancestral gene, and group I and group III genes are the results of duplications and transfer events (3).

At present, four trHbs from group I and two from group II have been structurally characterized (4–9). These studies revealed that specific residue deletions and substitutions distributed throughout the trHb sequence allow the achievement of the simplified fold, whereas granting enough affinity for the heme, and ligand access to the heme-iron atom. Among sequence peculiarities, two Gly-Gly sequence motifs have been deemed necessary for stabilization of the trHb fold in groups I and II, and identified in their related amino acid sequences (Fig. 1) (3, 4). Structural studies also showed that, in contrast to animal and plant globins, residues building the distal heme cavity of trHbs may vary considerably between groups and even

* This work was supported in part by Natural Sciences and Engineering Research Council of Canada Grant 46306-01 (2005–2010) and National Institutes of Health Grant 1-R01-AI052258 (2004–2007) (to M. G.) and the Italian Ministry for University and Scientific Research FIRB Project "Biologia Strutturale" Contract RBLA03B3KC (to M. B.). The costs of publication of this article were defrayed in part by the payment of page charges. This article must therefore be hereby marked "*advertisement*" in accordance with 18 U.S.C. Section 1734 solely to indicate this fact.

[S] The on-line version of this article (available at http://www.jbc.org) contains supplemental data, Figs. S1–S2, and Table S1.

The atomic coordinates and structure factors (code 2IG3) have been deposited in the Protein Data Bank, Research Collaboratory for Structural Bioinformatics, Rutgers University, New Brunswick, NJ (http://www.rcsb.org/).

[1] Supported by Centro Interdisciplinare Materiali e Interfacce Nanostrutturati (CIMAINA) (Milano, Italy) and Fondazione Cariplo (Milano, Italy). To whom correspondence should be addressed: Via Celoria 26, I-20131 Milano, Italy. Tel.: 39-02-50314893; Fax: 39-02-50314895; E-mail: martino.bolognesi@unimi.it.

[2] The abbreviations used are: trHb, truncated hemoglobin; Hb, hemoglobin; Mb, myoglobin; *Mt*-trHbN, *Mycobacterium tuberculosis* trHbN; *Mt*-trHbO, *Mycobacterium tuberculosis* trHbO; *Bs*-trHbO, *Bacillus subtilis* trHbO; *Cj*-trHbP, *Campylobacter jejuni* trHbP; r.m.s., root mean square.

between subgroups. Thus, except for the Phe(B9)[3]-Tyr(B10) pair commonly found, other residues lining the heme distal pocket are not conserved in trHbs. The proximal His(F8), which binds the heme iron, is the only truly invariant residues in trHbs (Fig. 1) (2, 3).

All trHbs investigated so far bind O_2, although with affinity ranging from nanomolar to micromolar. TrHbs from *Mycobacterium tuberculosis* (*Mt*-trHbN) and *Campylobacter jejuni* (*Cj*-trHbP) have been deeply investigated for their function. Studies performed with *Mycobacterium bovis* Calmette-Guerin (BCG) demonstrated that inactivation of the *glbN* gene impairs the ability of stationary phase cells to protect aerobic respiration from •NO inhibition, suggesting that trHbN may play a vital role in protecting *M. tuberculosis* from •NO toxicity *in vivo*. This functional assessment is supported by the observation that trHbN catalyzes the rapid oxidation of •NO into nitrate ($trHbN\text{-}Fe^{2+}O_2 + {}^{\bullet}NO \rightarrow trHbN\text{-}Fe^{3+} + NO_3^-$) with a second-order rate constant of 745 $\mu M^{-1}\,s^{-1}$ (10). *Mt*-TrHbN has also been shown to protect *Escherichia coli* against nitrosative stress (11). On the other hand, a trHbP defective *C. jejuni* was found disadvantaged with respect to wild-type cells when grown under high aeration, achieving lower growth yields and consuming O_2 at approximately half the rate displayed by wild-type cells. Interestingly, *Cj*-trHbP mutated cells did not show increased sensitivity to •NO or oxidative stresses. It has been proposed that *Cj*-trHbP may play a role in cell respiration (12, 13).

Inspection of the available group III trHb amino acid sequences (Fig. 1) indicates the absence of the Gly-Gly motifs, and a series of specific residue substitutions that fit only moderately on the sequence/structure scheme developed for groups I and II. On the other hand, analysis of 24 group III trHb amino acid sequences indicates a high level of residue conservation within this group, higher than within group I and group II trHbs (3). Based on the above considerations, the interest for structural characterization of a prototype group III trHb has grown substantially in the last few years, also considering that, in light of the sequence conservation reported above, it would allow generalization of structural properties to several of the known group III trHb sequences.

C. jejuni is a Gram-negative micro-aerophilic enteric microorganism, which is often the predominant pathogenic agent in bacterial gastrointestinal disease. It possesses two distinct hemoglobins encoded by the *Ctb* and *Cgb* genes, coding for a group III trHb, and a single domain "classic" globin, respectively (12, 13). In line with our continuous research activity on structure to function relationships in the trHb family, we present here the results of a crystallographic investigation on *C. jejuni* trHbP in its cyano-met form, at 2.15-Å resolution. We show that the main features of the trHb fold in *C. jejuni* trHbP are closer than expected to those observed for group II trHbOs. Structural features likely representative of group III trHbs are an extended C-helix, the presence of specific Trp residues, and the absence of a ligand diffusion protein matrix tunnel previously characterized in group I, and partly in group II trHbs. Our crystal structure suggests that ligand entry into the heme distal site is likely supported by the classical His(E7)-gating mechanism (14).

[3] Amino acid residues have been labeled using their three-letter codes, the sequence numbering (in parentheses), and the topological site they occupy within the globin fold; topological site identification has been omitted for most inter-helical residues.

EXPERIMENTAL PROCEDURES

Cloning, Expression, and Purification of Recombinant Cj-trHbP—Genomic DNA from *C. jejuni* NCTC11168 was kindly provided by Professor Sir Alec J. Jeffrey from University of Leicester (United Kingdom). We used the PCR to amplify the coding region of *Cj*-trHbP. The DNA primers used were (5′-CGCCTCCATATGAAATTTGAAACAATTAATC-3′, upper primer) and (5′-ATGGATCCAAAATTGCCAAATTAATG-TCC-3′, lower primer). The NdeI-BamHI digested PCR fragment was cloned into the pET3a prokaryotic expression vector and the recombinant protein was expressed in freshly transformed *E. coli* BL21(DE3). Cells were grown at 37 °C in 2-liter flasks containing 850 ml of Luria-Bertani medium containing 200 μg/ml ampicillin, 67 μg/ml of $FeCl_3$, and 10 μg/ml of hemin chloride until the absorption at 600 nm reached 0.5–0.8, at which point they were incubated for an additional 2 h. The cells were harvested by centrifugation at 5,000 × *g* for 15 min at 4 °C, and conserved at −80 °C. The cell pellet was resuspended with 0.02 volumes of 50 mM Tris-Cl, pH 7.5, buffer containing, 1 mM phenylmethanesulfonyl fluoride and DNase I (10 units/g). The cells were disrupted by passing them twice through a French pressure cell operated at 20,000 p.s.i., cooled at 4 °C. Cell debris were removed by centrifugation at 19,000 × *g* for 30 min at 4 °C. The extract was then fractionated with ammonium sulfate (40–80% saturation). The precipitate was centrifuged at 19,000 × *g* for 20 min, then resuspended in 10 mM Tris-Cl, pH 8.0, buffer containing 50 μM EDTA and dialyzed against the same buffer (3 times with 5 liters) overnight at 4 °C in 6–8-kDa molecular mass cutoff membranes (Spectrapor).

The dialysate was loaded onto a XK 26/40 column of 135 ml of DEAE-Sepharose Fast Flow (GE Healthcare), and the protein was eluted with a linear gradient (1350 ml) of 50–200 mM NaCl in 10 mM Tris-Cl, pH 8.0, buffer, containing 50 μM EDTA at 4 °C. Fractions with a 410/280 nm ratio >1.2 were pooled and concentrated by ammonium sulfate precipitation (95% saturation). The protein sample was then dissolved in 1–2 ml of 50 mM Tris-Cl, pH 7.5, buffer containing 50 μM EDTA, 300 mM NaCl, and dialyzed against the same buffer overnight at 4 °C. The protein sample was passed through a HiLoad 16/60 Superdex-75 gel-filtration column (prep grade, GE Healthcare) equilibrated with 50 mM Tris-Cl, pH 7.5, buffer containing 50 μM EDTA and 300 mM NaCl at 4 °C. Fractions with a 410/280 nm ratio >2.5 were pooled and concentrated by ammonium sulfate precipitation (95% saturation), and dialyzed against 10 mM Tris-Cl, pH 7.5, buffer containing 50 μM EDTA. The protein was oxidized using 10-fold molar excess potassium ferricyanide. After completion of the reaction, the protein was desalted over a phosphate-6-dehydrogenase (Bio-Rad) column equilibrated with 10 mM Tris-Cl, pH 7.5, buffer containing 50 μM EDTA.

For crystallographic studies the cyano-met form was obtained by incubating the protein with 10 mM KCN. The protein was then loaded onto a Resource Q 6-ml column (GE Healthcare) and eluted with a linear gradient (120 ml) of 0–200

TABLE 1
Data collection statistics for *Cj*-trHbP

	Space group	
	$P3_221$	$P2_1$
Cell dimensions	a = 95.6 Å, b = 95.6 Å, c = 65.4 Å	a = 68.3 Å, b = 39.5 Å, c = 68.6 Å, β = 102.8°
Resolution limits	65.94-2.15 Å	42.76-2.50 Å
Observations	274,246	43,327
Unique reflections	19,090	12,366
Completeness (%) overall (outer shell)	99.8 (100)	97.2 (96.5)
Mosaicity (°)	0.70	0.71
R_{merge}[a] (%) (outer shell)	6.7 (31.3)	8.6 (30.6)
$I/\sigma(I)$ (outer shell)	30.4 (8.9)	14.0 (3.8)
Multiplicity	14.4	3.5

[a] $R_{merge} = \Sigma_h\Sigma_i|I_{hi} - \langle I_h\rangle|/\Sigma_h\Sigma_i I_{hi}$.

TABLE 2
Refinement statistics and stereochemical analysis

	Space group	
	$P3_221$	$P2_1$
Refinement statistics		
Resolution range (Å)	31.3–2.15	40.0–2.5
R-factor[a]/R-free[b] (%)	20.6/26.2	21.9/26.6
Number of residues		
Monomer A	127	127
Monomer B	125	127
Number of heme groups	2	2
Number of cyanide ions	2	2
Number of acetate ions	2	
Number of sulfate ions	4	
Number of water molecules	93	15
Stereochemical analysis		
r.m.s. deviation from ideality		
Bond lengths (Å)	0.010	0.007
Bond angles (°)	1.130	1.041
Ramachandran plot		
Residues in most favored regions (%)	95.0	94.6
Residues in additional allowed regions (%)	5.0	5.4

[a] R-factor = $\Sigma_h||F_{obs}| - |F_{calc}||/\Sigma |F_{obs}|$, where F_{obs} and F_{calc} are the observed and calculated structure factor amplitudes, respectively.
[b] R-free is calculated on 10% of the diffraction data, which were not used during the refinement.

mM NaCl in 10 mM Tris-Cl, pH 7.5, buffer containing 10 mM KCN and 50 mM EDTA at 4 °C. Fractions with a 410/280 nm ratio >2.5 were pooled and concentrated by ammonium sulfate precipitation, as described above, and were dialyzed against 10 mM Tris-Cl, pH 7.5, buffer containing 50 μM EDTA overnight at 4 °C. The protein purity was assessed by SDS-PAGE. The heme was identified and quantified by the pyridine-hemochrome method.

Crystallization and Data Collection—Crystallization of *C. jejuni* trHbP was achieved using the hanging drop vapor diffusion setup. The protein solution, at 35 mg/ml concentration was equilibrated against a precipitant solution containing 2.0 M ammonium sulfate, 0.1 M sodium acetate, pH 4–5, at 277 K. Large single crystals grew within a few weeks. They were stored in a stabilizing solution containing 2.3 M ammonium sulfate, 0.1 M sodium acetate, pH 4–5, and then transferred to the same solution supplemented with 20% (v/v) glycerol, immediately prior to cryo-cooling and data collection. The crystals diffract up to 2.15-Å resolution, using synchrotron radiation (beamline ID29, ESRF, Grenoble, France), and belong to the trigonal $P3_221$, or $P3_121$, space group with unit cell parameters: a = 95.6 Å, b = 95.6 Å, c = 65.4 Å. The V_M value is 2.9 Å^3 Da^{-1}, with 57.1% solvent content, assuming two trHbP molecules (2 × 14937.2 Da). Alternatively, bunches of thin plates grew in about 2–3 weeks (each plate having typical dimensions of 0.3 × 0.2 × 0.005 mm^3) using a precipitant solution containing 2.0 M ammonium sulfate, 2.0 M NaCl, 50 mM KH_2PO_4, pH 6.5–7.5, at 277 K. The crystals were stored in a stabilizing solution containing 2.3 M ammonium sulfate, 2.0 M NaCl, 50 mM KH_2PO_4, pH 6.5–7.5; they were transferred to the same solution supplemented with 20% (v/v) glycerol, immediately prior to data collection (at 100 K). These crystals diffracted up to 2.5-Å resolution using synchrotron radiation (beamline ID14–3, ESRF, Grenoble, France), and were characterized as belonging to the monoclinic space group $P2_1$, with unit cell parameters: a = 68.3 Å, b = 39.5 Å, c = 68.6 Å, β = 102.8°. The V_M value is 3.0 Å^3 Da^{-1}, with 59% solvent content, assuming two trHbP molecules per asymmetric unit. All collected data were reduced and scaled using MOSFLM and SCALA, respectively (15, 16). Data processing statistics are reported in Table 1.

Structure Determination and Refinement—The structure was determined by molecular replacement using the program MolRep (17) as implemented in the CCP4 program package (18). The crystal structure of truncated group II trHbO from *Bacillus subtilis* (Protein Data Bank code 1UX8) (9) was used as search model, with side chains truncated to Ala in cases of mismatch between the two amino acid sequences. The rotational and translational searches run in the 40–3.5-Å resolution range yielded a prominent solution for a dimeric molecule (solving the space group ambiguity in favor of $P3_221$). After rigid body refinement of this solution (moving independently all the helices and the heme group in each monomer), the final correlation coefficient and R-factor values were 30.0 and 50.2%, respectively (at 2.15-Å resolution). Several cycles of manual rebuilding, using the program O (19), and refinement, using the program REFMAC (20) (rigid body and restrained refinement), were carried out to improve the electron density map, and model the protein loops that were not visible in the initial maps. At the end of the refinement stages, 93 water molecules, 2 acetate, and 4 sulfate ions were located through inspection of difference Fourier maps, using the program O. The final R-factor value was 20.6% and R-free 26.2% (Table 2).

The refined structure of *Cj*-trHbP was then used as a starting model to solve the structure and refine the $P2_1$ crystal form, following the same procedures described above. At the end of the refinement stages, 15 water molecules were located through inspection of difference Fourier maps, using the program O. The final R-factor value was 21.9% and R-free 26.6% (Table 2).

The programs Procheck (21) and Surfnet (22) were used to assess the stereochemical quality of the protein structures and explore the protein matrix cavities. The program PISA (23) was used to identify putative quaternary assemblies within the crystal unit cell. Atomic coordinates and structure factors have been deposited with the Protein Data Bank (24), with entry codes 2IG3 and r2IG3sf, respectively.

RESULTS AND DISCUSSION

Quality of the Model—The structure of *Cj*-trHbP was solved on crystals belonging to the trigonal space group $P3_221$ (two molecules per asymmetric unit, referred to as A and B, respectively) by means of molecular replacement, based on the model

of group II trHbO from *B. subtilis* (PDB code 1UX8) (9). The *Cj*-trHbP structure was refined at 2.15-Å resolution, to final *R*-factor and *R*-free values of 20.6 and 26.2%, respectively, with ideal stereochemical parameters (Table 2). His[46](E7) displays a double conformation in chain B; additionally, in this chain no electron density is observed for the last two C-terminal residues. Superposition of 122 C_α atoms of the two independent *Cj*-trHbP chains (excluding the last C-terminal 5 residues) yields a r.m.s. deviation of 0.43 Å. All results discussed below apply to both chains A and B unless otherwise stated.

Additionally, crystals of the *Cj*-trHbP, grown in the $P2_1$ space group (two molecules per asymmetric unit), were also analyzed and refined against a 2.5-Å resolution data set, yielding *R*-factor and *R*-free values of 21.9 and 26.6%, respectively, with ideal stereochemical parameters (Table 2). Superposition of 127 C_α atoms of the two independent molecules yields a r.m.s. deviation of 0.19 Å. Comparison of the *Cj*-trHbP structures from the monoclinic and trigonal crystal forms yielded r.m.s. deviations in the 0.36–0.38-Å range, for 122 C_α atoms (excluding the last C-terminal 5 residues), depending on the chains superposed.

Overall Structural Properties—*Cj*-trHbP shows the typical features of the 2-on-2 α-helical trHb-fold (2, 4–9), described as a subset of the classical globin 3-on-3 α-helical sandwich (25, 26) (Figs. 1 and 2). Structural superpositions (limited to 68 C_α atoms of the B, E, F, G, and H helices, Fig. 2) of *Cj*-trHbP with the known structures of group I and II trHbs (4, 5, 7–9) yield r.m.s. deviations in the 1.05–1.35-Å range.

Despite the considerable divergence evident in the amino acid sequences of the whole trHb family (Fig. 1), the above comparative structural analysis stress the conservation of the 2-on-2 trHb fold, but it also highlights some key structural properties of group III proteins. Among these, helix A is completely absent in *Cj*-trHbP, and the N-terminal backbone runs, in an extended conformation, in the opposite direction relative to the corresponding region in group I and II trHbs (Fig. 2, *B* and *C*). Such peculiar orientation of the *Cj*-trHbP pre-B region is supported by hydrogen bonding interactions between Phe[3] O–Asn[99] NH, Phe[3] NH–Val[97](G19) O, and Lys[2] NZ–Asn[95](G17) O atoms, being structurally related to the absence of Gly-Gly sequence motifs at the AB and EF interhelical hinges of group III trHbs (supplemental materials Fig. S1A). Given that the observed conformation of the pre-A region is stabilized by three hydrogen bonds in an otherwise solvent-exposed environment, additional conformations dynamically accessible to this N-terminal region cannot be excluded (6). The Gly-based motifs are instead conserved, and are key sequence markers, in group I and II trHbs (Fig. 1) (2, 3), where they help stabilize the short A helix in a conformation locked onto helices B and E (supplemental materials Fig. S1B) (4, 5). In *Cj*-trHbP such a stabilizing interaction is lost because the first residue of the modified Gly-Gly motif in the EF hinge is Leu[59], whose side chain fills the spatial location occupied by the side chain of Tyr/Phe A12 in group I and II trHbs (supplemental materials Fig. S1). However, stabilizing interactions between the B and E helices are granted by an extended distribution of hydrophobic residues at the B/E helical interface (supplemental materials Fig. S1A). Furthermore, the absence of the Gly-Gly motif at the AB hinge of *Cj*-trHbP does not provide the backbone flexibility required to direct the N terminus toward the BE interhelical region, thus forcing the protein residues preceding the B helix to extend toward the GH region.

A unique structural feature of group III trHbs is a 3–7-amino acid insertion located between the C and E helices (Fig. 1). Surprisingly, such elongation of the CD region in *Cj*-trHbP does not shift the position of helix E relative to the heme distal site. Rather, it affects the span of the C and E helices, which relative to the corresponding helices in group I and II trHb structures, gain one C-terminal and one N-terminal turn, respectively (Fig. 2, *B* and *C*). Thus, the protein structure in the short region comprised between the C and E helices deviates markedly (up to 7.5 Å) in the three trHb groups. Additionally, in *Cj*-trHbP the C helix displays a clear α-helical character, as compared with the 3_{10} helical character commonly displayed not only by group I and II trHbs but also by vertebrate globins (14). Interestingly, juxtaposition of the C and E helices is granted by a bifurcated hydrogen bond connecting the group III conserved Trp[43](E4) NE1 to Asn[33] OD1, and to Gly[37] O; the Trp[43](E4) indole side chain is shielded from the solvent region by the Arg[23](B14) NH1–Asp[40](E1) OD1 salt bridge.

Additional regions of structural deviation in the group III trHb fold are the *Cj*-trHbP EF and FG hinge regions, as partly suggested by their amino acid sequences diverging from those of group I and II trHbs (Fig. 1). In particular, the EF hinge does not host the short α-helical segment found in group II trHbs, and its extended conformation is markedly different from that of group I *Paramecium caudatum* trHbN, *Chlamydomonas eugametos* trHbN (4), and *Synechocystis* trHbN (6, 8), being more similar to *M. tuberculosis* trHbN (5) (Fig. 2, *B* and *C*). The FG hinge structure in *Cj*-trHbP is dominated by the presence of three proline residues (PPFP motif, Fig. 1). These define the extended (and rigid) conformation of the hinge, having as a consequence the partial unwinding of the first turn of the G helix, and marked separation between the G and H helices in its surroundings. Helix H is unusually long in *Cj*-trHbP (24 residues); it does not show any C-terminal kink, typical of group I trHbs (27), or shortening, as found in group II *Mt*-trHbO (7) and *Bs*-trHbO (9) (Fig. 2, *B* and *C*).

Contrary to what has been observed in group I and II trHbs (2, 28), inspection of the overall *Cj*-trHbP structure shows no evident protein matrix tunnel/cavity system, as defined by a 1.4-Å radius probe. If a smaller probe is used (1.2-Å radius), two minor hydrophobic cavities (about 15-Å^3 volume) can be identified. One is lined by hydrophobic residues contributed by helices B, G, and H; the other is lined by Met[15](B6), Phe[18](B9), Tyr[19](B10), Ile[50](E11), Trp[54](E15), Trp[86](G8), and Phe[90](G12), being located between the first cavity and the heme distal site. Interestingly, the second cavity hosts a water molecule that acts as a hydrogen-bond bridge between the heme distal residues Tyr[19](B10) (OH group) and Trp[54](E15) (NE1 atom) (Fig. 3). The first cavity located in *Cj*-trHbP falls in the topological region hosting the protein matrix tunnel long branch in group I and II trHbs, but it is not open to the heme distal site, nor to the solvent space.

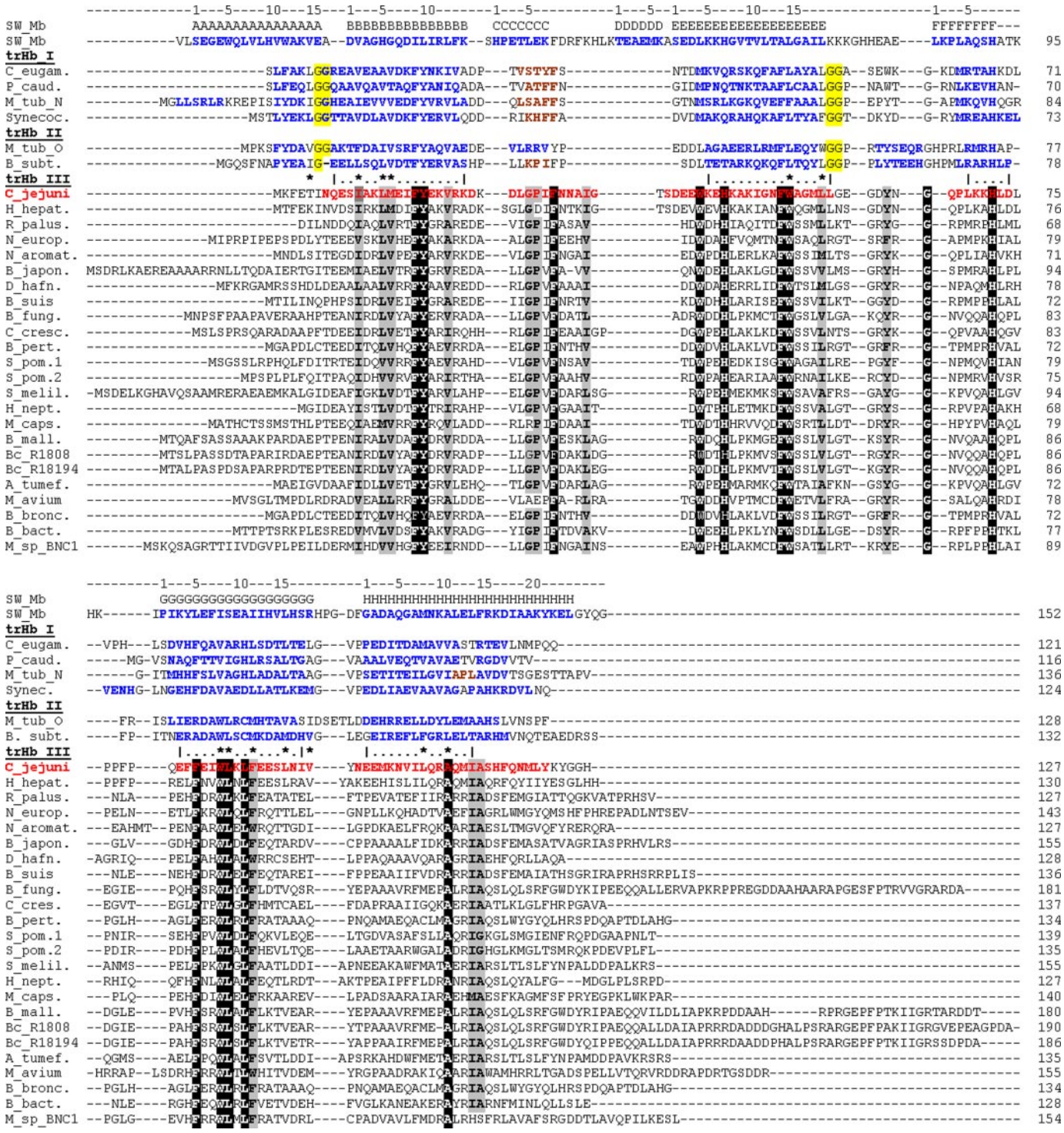

FIGURE 1. **Structure-based sequence alignment of *Cj*-trHbP with members of groups I, II, and III of the trHb family.** The globin fold topological positions, as defined in sperm whale Mb, are shown on the *top* of the sequence alignment. α-Helical and 3_{10} regions are highlighted in *blue* and *brown*, respectively (*red* for *Cj*-trHbP), and residues used for Cα superimposition are indicated by | . . . | segments. Residues that are conserved or similar in group III trHbs are highlighted in *black* and *gray boxes*, respectively; *yellow bars* highlight the Gly-Gly motifs conserved in group I and II trHbs. Residues corresponding to those lining the group I trHbs apolar protein tunnel are marked with *asterisks*. Sequences have been selected based on Vuletich and Lecomte (3).

Aggregation State of Cj-trHbP—Two *Cj*-trHbP chains (A and B) are present in the crystallographic asymmetric unit of both $P3_221$ and $P2_1$ crystal forms; however, the putative dimers found in different crystal packing contexts display different and unrelated quaternary structures. Moreover, only the $P3_221$ dimer, which has a subunit contact interface of ~860 Å^2 (corresponding to ~10.5% of the total surface of each monomer), is predicted energetically stable by the Protein Interfaces, Surfaces and Assemblies (PISA) detection software (23). The $P2_1$ dimeric form (~475 Å^2 of buried interaction interface, corresponding to only ~6% of the total monomer surface) does not reveal specific interactions that could suggest the formation of a

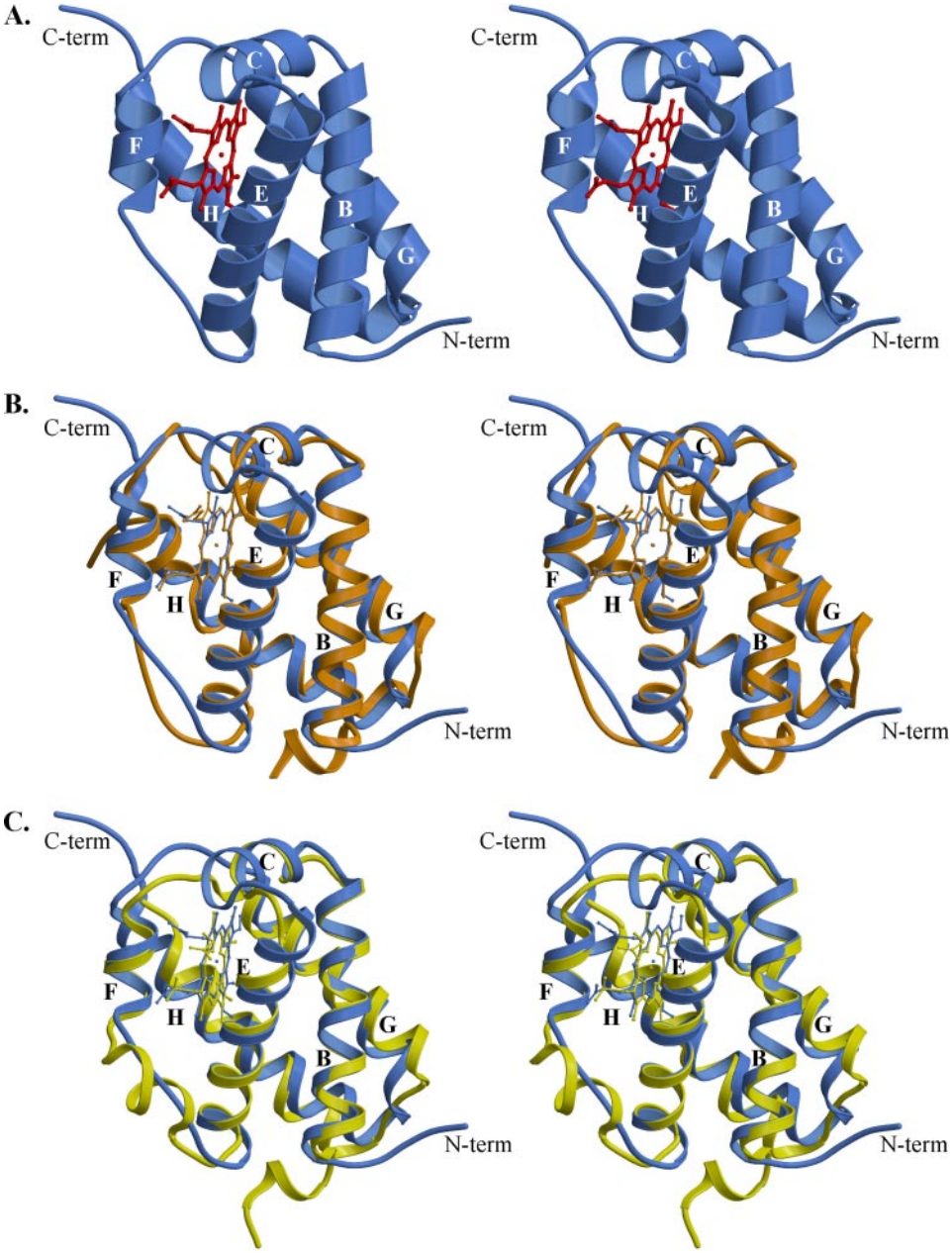

FIGURE 2. **A comparative view of the trHb fold in the three groups.** *A*, a ribbon stereo view of *Cj*-trHbP tertiary structure. α-Helices are labeled according to the conventional globin fold nomenclature (25). *B*, structural overlay of group III *Cj*-trHbP (*blue trace*) onto group I *C. eugametos* trHbN (*orange trace*). *C*, structural overlay of group III *Cj*-trHbP (*blue trace*) onto group II *B. subtilis* trHbO (*yellow trace*). The heme groups of each globin are included. All figures were drawn with Molscript (33) and Raster3D (34).

stable assembly. Indeed, gel filtration experiments show that the protein elutes as a monomer (13).[4] Taken together, these results strongly suggest that the observed putative dimeric forms are induced by the high protein concentration achieved during crystallization rather than being functional quaternary assemblies.

Heme Stabilization and the Heme Proximal Site—Inspection of the electron density indicates that in both *Cj*-trHbP chains the heme group is rotated by 180° along the methinic α-γ meso axis, relative to the majority of (non)-vertebrate globins (25). Selection of the orientation of the heme can be related to the specific location of the G and H helices relative to the heme crevice, and to specific heme-protein contacts at residues Trp[86](G8) and Ala[114](H15), as found for group II *Mt*-trHbO (7) and for *Bs*-trHbO (9). Stabilization of the bound heme in *Cj*-trHbP is achieved through direct iron coordination to the proximal His[72](F8) residue, electrostatic interaction of the heme propionates, and van der Waals contacts (<4.0 Å) with 22 protein residues. A hydrogen-bonded salt bridge to Lys[49](E10) is provided by the heme propionate D (Fig. 3). Furthermore, Lys[71](F7) falls at 4–4.5 Å from both propionates A and D in monomer A, whereas it makes a hydrogen-bonded salt bridge to propionate D, in chain B. This difference between the two *Cj*-trHbP monomers is related to variation of the hydrogen bonding pattern around the heme propionates induced by different conformations of the distal His[46](E7) (see below). Residue E10 is strongly conserved as Arg/Lys in all three trHb groups, whereas Arg at position F7 is invariant in group II trHbs (Fig. 1) (2, 3). Additionally, propionate D is hydrogen bonded to Tyr[64] (pre-F region), which is strongly conserved in group III trHb (Fig. 2). A similar heme stabilizing interaction is present in group I trHbNs from *M. tuberculosis* (3) and from *Synechocystis* (8), and in group II trHbOs from *M. tuberculosis* (7) and *B. subtilis* (9) (Fig. 2).

The architecture of the heme pocket in the proximal region is dominated by Pro[68](F4), Leu[75](FG3), Phe[78], Phe[83](G5), and Phe[117](H18), all of which contact the porphyrin ring. The position and orientation of the proximal His[72](F8) is typical of an unstrained imidazole ring that facilitates the heme in-plane location of the iron atom (Fig. 3*A*). Analysis of the stereochemical parameters describing the heme iron coordination indicates a regular iron-His(F8) NE2 coordination bond (2.09 Å, averaged over the 2 subunits) (25), with the imidazole plane lying in a staggered orientation relative to the heme pyrrole N-atoms, thus increasing covalence of the iron–His(F8) bond. Such proximal His-staggered orientation is in agreement with the observed iron-His stretching frequency observed values (226 cm^{-1}) (13).

[4] M. Nardini, A. Pesce, M. Labarre, C. Richard, A. Bolli, P. Ascenzi, M. Guertin, and M. Bolognesi, unpublished data.

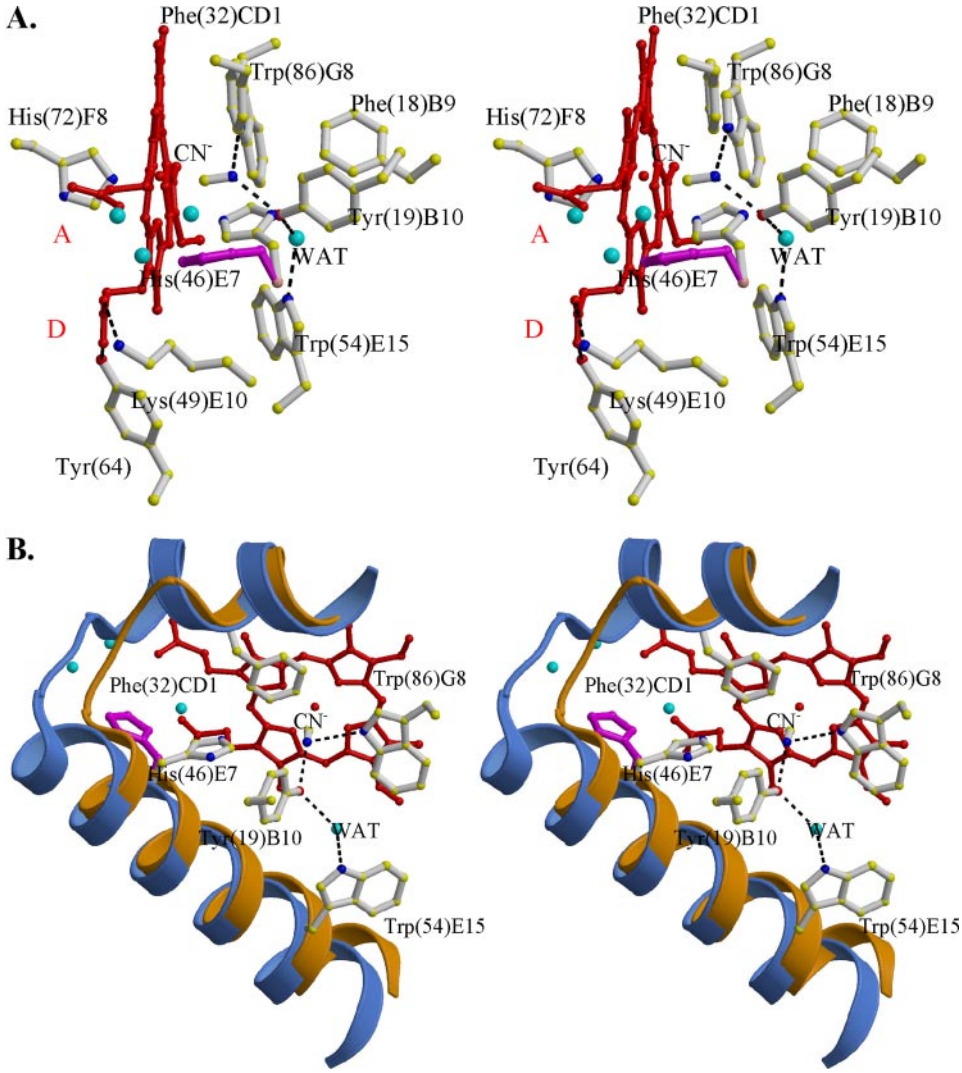

FIGURE 3. **Structure in the heme pocket of *Cj*-trHbP.** *A*, a stereo view of the heme, of the proximal His(F8), and of the surrounding distal residues contacting the heme and stabilizing the bound cyanide. Hydrogen bonds within the distal residue cluster, including the heme ligand, are indicated with *dashed lines*. Residue His[46](E7) is shown in the closed and open (*magenta*) conformations. *B*, details of the heme distal site, including the C helix (*top* in the figure) and the E helix; for comparison, the C-E backbone region of group I *C. eugametos* trHbN (*orange*) is also displayed. Water molecules are shown as small (*cyan*) spheres in both panels, with the water molecule located in the internal small protein cavity indicated by "WAT."

The solvent side of the proximal heme pocket is largely occupied by Lys[71](F7), which, being electrostatically coupled to the heme propionates, effectively shields His[75](F8) from the solvent. The *Cj*-trHbP structure, therefore, differs from group II *Mt*-trHbO and *Bs*-trHbO, where the heme proximal residue is directly exposed to solvent through an aperture (45–55 Å^2) situated in a shallow depression next to the F7 residue (9).

Analysis of surface accessibility (1.4-Å radius probe) shows the presence of two surface crevices around the heme proximal side, one of which is localized between the C helix and the PPFP motif (in the FG hinge) (Fig. 1). The second crevice falls between the FG segment and the C terminus of the H helix. Both crevices point to the heme pocket from the solvent region, being separated from the proximal site by residue gates built by Ile[31](G7)-Phe[78] and by Phe[78]-Leu[121](H21), respectively. In addition, inspection of the protein surface shows that the region built by the pre-F loop and the H helix shield the heme C and D pyrrole rings essentially by virtue of residue Phe[53](E14), which is invariant through the three trHb groups (Fig. 1). Small conformational fluctuations at Phe[53](E14), located at the center of a low polarity surface region, can open the proximal heme cavity to small diatomic molecules or to the solvent.

Heme Distal Pocket—The heme distal pocket residues Phe[18](B9), Tyr[19](B10), Phe[32](CD1), His[46](E7), Ile[50](E11), Phe[52](E14), and Trp[86](G8) surround the heme-bound ligand in *Cj*-trHbP (Fig. 3*A*). Most of these residues are conserved in more than one trHb group, with the exception of His[46](E7), which is fully conserved only in group III (Fig. 1). Within the distal cavity, Tyr[19](B10) plays a pivotal role in ligand stabilization by hydrogen bonding through its OH group directly to the cyanide N atom (2.71 Å). The cyanide ligand is nearly perpendicular to the heme plane, with a iron–C coordination bond of 1.91 Å. Additionally, ligand stabilization (through hydrogen bonding) is provided by the indole NE1 atom of Trp[86](G8), which is at 3.26 Å from the cyanide N atom (all reported distances have been averaged over the two protein chains). At the dead end of the distal pocket, Trp[86](G8), conserved in trHb groups II and III, fills the inner part of the heme distal site, preventing the diffusion of ligands away from the iron coordination site. Trp[86](G8) indole ring is parallel and in contact with the heme plane at the B and C pyrrole rings (Fig. 3, *A* and *B*).

The *Cj*-trHbP cyanide binding mode is reminiscent of that found in group II *Bs*-trHbO (9), with good residue conformation matching for Tyr(B10) and Trp(G8). Moreover, the water molecule found bridging residues Tyr(B10) and Trp(E15) (filling the second small matrix cavity) matches the site occupied by the Gln[49](E11) OE1 atom in *Bs*-trHb, but it is not in contact with the bound cyanide, contrary to what is observed for the *Bs*-trHb Gln[49](E11) OE1 atom (9). When compared with group I trHbs, the *Cj*-trHbP cyanide binding mode mostly resembles that found in *Mt*-trHbN (29), with differences due to substitutions in the latter protein of residues Val and Gln at sites G8 and E11, respectively. Notably, the *Mt*-trHbN Gln(E11) side chain partly matches the *Cj*-trHbP water molecule bridging Tyr[19](B10) OH and Trp[54](E15) NE1 atoms.

Due to the increased extension of the C helix observed in *Cj*-trHbP, residue Ile[36], which would formally be assigned to

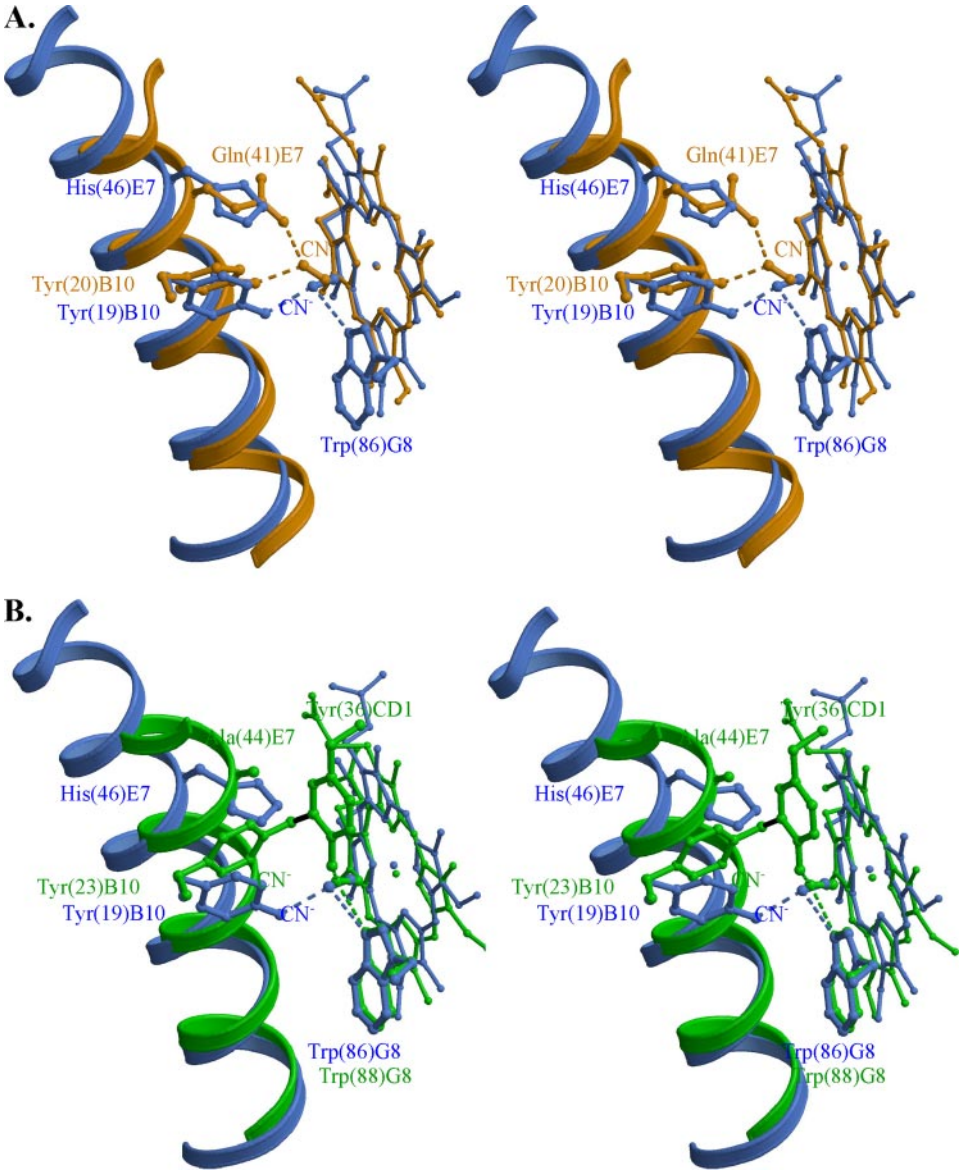

FIGURE 4. **Different orientation of the E helix in trHbs.** *A*, a stereo view of the superimposition of *Cj*-trHbP (*blue*) with group I *C. eugametos* trHbN (*orange*) in an orientation highlighting hydrogen bonds (*dashed lines*) between the bound cyanide and the protein distal residues. *B*, superimposition of *Cj*-trHbP (*blue*) with group II *M. tuberculosis* trHbO (*green*). The covalent bond linking Tyr^{23}(B10) and Tyr^{36}(CD1) is shown as a *continuous black line*.

the topological CD4 site, is indeed still part of the C helix (in practice the "C11" topological site, within the globin fold), and contributes to shield the heme distal face together with Ala^{35}(CD3). Conversely, residue Phe^{32}(CD1) falls roughly in the middle part of the C helix; such a location of PheCD1, central within the C helix, is observed in *Cj*-trHbP for the first time relative to all known globin structures (Figs. 1 and 3*B*).

Lys^{49}(E10), a well conserved positively charged residue in all three trHb groups, forms a salt bridge at the outer rim of the distal site, with the heme propionate D (O1D–NZ distance of 2.91 Å; Fig. 3*A*). This salt bridge is on the external surface of the protein and may partly hinder access to the distal pocket. However, due to the extended C helix, room is available to grant solvent access to the distal site through the E7-gate path. Indeed, analysis of the surface accessibility, using a 1.4-Å radius probe, shows that His^{46}(E7) is solvent accessible through a crevice localized between the Ile^{36}, Glu^{42}(E3), Lys^{49}(E10), and Glu^{45}(E6) side chains, and the heme propionate A. In keeping with such observations, the crevice hosts four and three water molecules in chains A and B, respectively. Furthermore, in chain B, His^{46}(E7) is present in two alternate conformations, "open" and "closed" (both refined to 0.50 occupancy) corresponding to the His^{46}(E7) side chain pointing toward the solvent or to the heme distal site, respectively (Fig. 3, *A* and *B*). The open conformation is stabilized by a hydrogen bond between the His^{46}(E7) ND1 atom and Glu^{42}(E3) carbonyl O, whereas a similar interaction to the Glu^{42}(E3) O atom is granted in chain A by the presence of a water molecule substituting for the ND1 atom of the open His^{46}(E7). In the closed conformation, His^{46}(E7) is not involved in any polar contact with protein atoms nor with the ligand, being more than 4 Å away from both the Tyr^{19}(B10) OH group and the cyanide N atom (Fig. 3*B*). Such a distal site arrangement differs from the cyanide stabilization mode observed in sperm whale Mb, where the gating-residue His(E7) is also actively involved in locking the heme-Fe(III)-bound cyanide in the heme distal site through hydrogen bonding (30). This behavior can be related in sperm whale Mb to the presence of helix D (Fig. 1), which positions helix E in an orientation much closer to the heme than in *Cj*-trHbP. As a consequence, when superimposing the proximal His residue and the heme group of sperm whale Mb and *Cj*-trHbP, the His(E7) C_α atoms of the two proteins fall 5.2 Å apart, the heme distal residue of *Cj*-trHbP being farther away from the heme, with no possibility to contact directly with the heme-coordinated ligand. A similar dislocation of the His(E7) residue is observed when *Cj*-trHbP is compared with group I and II trHbs; for instance, due to the elongated C-helix, the distal His^{46}(E7) C_α atom falls about 1.1 and 1.9 Å farther away from the heme iron atom relative to the same C_α-Fe distance in *C. eugametos* trHbN and *M. tuberculosis* trHbO (Fig. 4).

Structural-based Sequence Analysis in trHb Group III—Cj-trHbP displays sequence identity in the 20–33% range relative to other members of trHb group III; the only presently known exception is *Helicobacter hepaticus* trHbP, whose sequence is about 66% identical to that of *Cj*-trHbP. Inspection of amino acid sequence alignments based on the present crystal structure

allows identifying several residues conserved at key structural positions (Fig. 1). The number of conserved residues appears to be higher in group III than in group I or II trHbs, as pointed out by Vuletich and Lecomte (3) based on their recent sequence analysis. *Cj*-trHbP, the first three-dimensional structure to be reported for group III trHbs, therefore appears to be a good prototypic structural model for the whole group III.

Analysis of sequences in light of the three-dimensional structure shows that a pronounced level of sequence identity/similarity is located within the secondary structure elements, mostly associated to residues building the proximal and distal site heme pockets, or involved in heme stabilization (Fig. 1). In particular, a strong conservation of the distal site residues appears evident. In fact, the full conservation of residues Phe(B9), Tyr(B10), Phe(CD1), His(E7), Trp(G8), and Trp(E15) may translate for most trHbPs into ligand recognition principles closely matching those of *Cj*-trHbP, where, similarly to group II trHbs, the cyanide ligand is primarily stabilized by hydrogen bonds to Tyr(B10) OH and to the Trp(G8) indole NE1 atoms. It is worth recalling that a distal site hydrogen-bonding network, based on group-specific distal residues, is a constant structural property of trHbs (2, 4–9, 27).

Residue conservation around the heme is also evident for residues Pro(F4), Leu(FG3), Phe(G5), and His(F8), on the proximal side, and extends to several residues involved in heme stabilization through van der Waals contacts, such as Leu(C4), Ile(C7), Phe(CD1), Ile^{36}, Phe(G5), Ile(E11), Phe(E14), Trp(E15), Pro(F4), Leu(FG2), Phe(FG6), Ile(H14), Ala(H15), and Phe(H18), or through polar contacts, such as Lys(E10) and Tyr^{64} (from the pre-F region) (Fig. 1). It should be noted that Lys(F7), despite being involved in electrostatic stabilization of the heme in *Cj*-trHbP, is not conserved in trHb group III, whereas Arg at position F7 is invariant in group II trHbs, and plays a comparable heme stabilizing role (Fig. 1) (5). A low level of sequence conservation is instead found for residues lining the two crevices that may provide access to the *Cj*-trHbP heme cavity from the proximal side. In view of the reported sequence variability, these putative proximal access routes are likely to be a structural feature unique to *Cj*-trHbP.

The previous crystallographic and sequence analyses on group I and group II trHbs highlighted two Gly-Gly sequence motifs, located at the AB inter-helical hinge, and C-terminal to the E helix, respectively, as fingerprints of the trHb fold. Additionally, one conserved Gly residue was identified six residues downstream of the second Gly-Gly motif (3–5). Inspection of the *Cj*-trHb structure and group III trHb sequences shows that the last Gly residue is conserved in group III trHb, and an additional single Gly four residues downstream is also highly conserved in group III, but not in group I and II trHbs. On the contrary, an evident feature of group III trHbs is the absence of the two AB and EF inter-helical hinge Gly-Gly motifs. Based on the results here presented for the *Cj*-trHbP structure, it must be concluded that the latter motifs are not essential to preserve the main features of the 2-on-2 trHb fold.

The absence of Gly-Gly motifs in group III trHbs is, however, reflected by a peculiar structure of the pre-B helix residues (the N terminus in *Cj*-trHbP), and correlates with obstruction of the protein matrix tunnel observed in group I trHbs. In fact, bulky side chain substitutions at residues lining the tunnel/cavities walls in group I and II trHbs are evident and conserved within group III members at topological site B5, at site E15, where a group III invariant Trp substitutes for the tunnel-gating residue Phe(E15) present in group I tr-HbN, and at sites G8, G9, GH6, G12, and partly in H12 (Fig. 1). Thus, the structural analysis of *Cj*-trHbP allows us to conclude that the protein tunnel/cavity system detailed for group I trHbs (5, 27) is not likely to be a prominent structural feature conserved in group III trHbs. On the other hand, the constant presence of a (3–7 residue) sequence insertion localized between the C and E helices, and a good sequence similarity at sites E3, E6, and E10, suggest that the solvent accessibility of the distal HisE7 residue, and its ligand gating role proposed for *Cj*-trHbP, may be a general feature of group III trHbs.

CONCLUSIONS

The three-dimensional structure of *Cj*-trHbP provides the first insights on the fold and ligand recognition properties of group III trHbs. Despite the low sequence identity to trHbs from groups I and II, the tertiary structure based on a 2-on-2 α-helical sandwich is maintained in group III proteins. In particular, the absence of the two Gly-Gly motifs, conserved at the AB and EF inter-helical hinges in group I and II trHbs, shows that these motifs are dispensable for the achievement and stabilization of the trHb fold. Their absence is reflected by evident structural changes localized: (i) at the N terminus, where helix A is completely absent and the backbone runs in a direction opposite to that observed in the known group I and II trHbs; and (ii) at the EF hinge, whose extended conformation does not match that of group I trHbs, nor the short α-helical segment found in group II trHbs.

Careful reshaping of the 2-on-2 fold, together with selected side chain substitutions, is in keeping with obstruction (or constriction) of the protein matrix tunnel connecting the solvent region to the heme distal pocket most prominently in group I trHbs. Thus, taken together, the known crystal structures from trHbs of the three groups support the idea of a conserved 2-on-2 α-helical sandwich fold that has intrinsic potential for the formation of protein-matrix cavities that, however, may or may not lead to functional cavity/tunnel system(s) (linking the solvent space to the heme) depending on specific residue substitutions and local backbone rearrangements. When a cavity/tunnel system is absent, alternative heme distal site access may be granted through other routes, for instance through the exposed 8-methyl edge of the heme group and near the propionates, as proposed for the hexacoordinated trHbN from *Synechocystis* (6), or by a "classical" gating role of the His(E7) side chain (31, 32), as suggested by the structure of *Cj*-trHbP. In this respect, it is remarkable that dissociation of cyanide from ferrous *Cj*-trHbP (as detailed in the associated supplemental data) is a slow process (the kinetic rate constant being $k_{off} = 5 \times 10^{-3}$ s^{-1}, see supplemental materials Table S1), and comparable with what has been observed for group I and II trHbs. Such observation suggests that energetically equivalent mechanism(s) may be involved in the stabilization of the heme-bound cyanide, and/or in the protonation of the outgoing ligand, despite evi-

dent variations in the stabilization of the heme-bound cyanide in different trHbs (29).

In general terms, the data presented here complete the structural picture of the trHb family, which is now fully represented in its three groups. Despite such progress, the specific function of trHbs *in vivo* remains an open issue, with the only exception of the NO scavenging function assigned to *M. tuberculosis* trHbN (10, 11), and the putative roles in moderating O_2 consumption, or in facilitating O_2 transfer proposed for *Cj*-trHbP (12, 13). Generic O_2 binding properties can be assigned to all trHbs, in consideration of the stereochemistry (or residue composition) of their heme distal sites, and of ligand recognition stereochemical principles, based on the available crystal structures. The widely different ligand (*e.g.* O_2) binding parameters, which are currently known only for a limited set of trHbs, suggest that very different functions may be displayed by these globins in their natural environments. It is remarkable how such proposed functional variability may be hosted by the trHb protein chains, which are definitely smaller than those of classical (non)vertebrate globins whose *in vivo* functions are held to be less differentiated.

REFERENCES

1. Vinogradov, S. N., Hoogewijs, D., Bailly, X., Arredondo-Peter, R., Guertin, M., Giugh, J., Dewilde, S., Moens, L., and Vanfleteren, J. R. (2005) *Proc. Natl. Acad. Sci. U. S. A.* **102,** 11385–11389
2. Wittenberg, J. B., Bolognesi, M., Wittenberg, B. A., and Guertin, M. (2002) *J. Biol. Chem.* **277,** 871–874
3. Vuletich, D. A., and Lecomte, J. T. (2006) *J. Mol. Evol.* **62,** 196–210
4. Pesce, A., Couture, M., Dewilde, S., Guertin, M., Yamauchi, K., Ascenzi, P., Moens, L., and Bolognesi, M. (2000) *EMBO J.* **19,** 2424–2434
5. Milani, M., Pesce, A., Ouellet, Y., Ascenzi, P., Guertin, M., and Bolognesi, M. (2001) *EMBO J.* **20,** 3902–3909
6. Falzone, C. J., Vu, B. C., Scott, N. L., and Lecomte, J. T. (2002) *J. Mol. Biol.* **324,** 1015–1029
7. Milani, M., Savard, P. Y., Ouellet, H., Ascenzi, P., Guertin, M., and Bolognesi, M. (2003) *Proc. Natl. Acad. Sci. U. S. A.* **100,** 5766–5771
8. Trent, J. T., 3rd., Kundu, S., Hoy, J. A., and Hargrove, M. S. (2004) *J. Mol. Biol.* **341,** 1097–1108
9. Giangiacomo, L., Ilari, A., Boffi, A., Morea, V., and Chiancone, E. (2005) *J. Biol. Chem.* **280,** 9192–9202
10. Ouellet, H., Ouellet, Y., Richard, C., Labarre, M., Wittenberg, B., Wittenberg, J., and Guertin, M. (2002) *Proc. Natl. Acad. Sci. U. S. A.* **99,** 5902–5907
11. Pathania, R., Navani, N. K., Gardner, A. M., Gardner, P. R., and Dikshit, K. L. (2002) *Mol. Microbiol.* **45,** 1303–1314
12. Wainwright, L. M., Elvers, K. T., Park, S. F., and Poole, R. K. (2005) *Microbiology* **151,** 4079–4091
13. Wainwright, L. M., Wang, Y., Park, S. F., Yeh, S. R., and Poole, R. K. (2006) *Biochemistry* **45,** 6003–6011
14. Bolognesi, M., Bordo, D., Rizzi, M., Tarricone, C., and Ascenzi, P. (1997) *Prog. Biophys. Mol. Biol.* **68,** 29–68
15. Leslie, A. G. M. (2003) *MOSFLM User Guide*, Mosflm Version 6.2.3, MRC Laboratory of Molecular Biology, Cambridge, UK
16. Evans, P. R. (1993) *Proceedings of the CCP4 Study Weekend on Data Collection and Processing*, pp. 114–122, CLRC Daresbury Laboratory, UK
17. Vagin, A., and Teplyakov, A. (1997) *J. Appl. Crystallogr.* **30,** 1022–1025
18. Collaborative Computational Project, Number 4 (CCP4) (1994) *Acta Crystallogr. Sect. D Biol. Crystallogr.* **50,** 760–763
19. Jones, T. A., Zou, J. Y., Cowan, S. W., and Kjeldgaard, M. (1991) *Acta Crystallogr. D Biol. Crystallogr.* **47,** 110–119
20. Murshudov, G. N., Vagin, A. A., and Dodson, E. J. (1997) *Acta Crystallogr. D Biol. Crystallogr.* **53,** 240–255
21. Laskowski, R. A., MacArthur, M. W., Moss, D. S., and Thornton, J. M. (1993) *J. Appl. Crystallogr.* **26,** 283–291
22. Laskowski, R. A. (1995) *J. Mol. Graph.* **13,** 323–330
23. Krissinel E., and Henrick K. (2005) in *Detection of Protein Assemblies in Crystals* (Berthold, M. R., Glen, R., Diederichs, K., Kohlbacher, O., and Fischer, I., eds) CompLife 2005, LNBI 3695, pp. 163–174, Springer-Verlag, Berlin
24. Berman, H. M., Westbrook, J., Feng, Z., Gilliland, G., Bhat, T. N., Weissig, H., Shindyalov, I. N., and Bourne, P. E. (2000) *Nucleic Acids Res.* **28,** 235–242
25. Perutz, M. F. (1979) *Annu. Rev. Biochem.* **48,** 327–386
26. Holm, L., and Sander, C. (1993) *FEBS Lett.* **315,** 301–306
27. Milani, M., Pesce, A., Nardini, M., Ouellet, H., Ouellet, Y., Dewilde, S., Bocedi, A., Ascenzi, P., Guertin, M., Moens, L., Friedman, J. M., Wittenberg, J. B., and Bolognesi, M. (2005) *J. Inorg. Biochem.* **99,** 97–109
28. Milani, M., Pesce, A., Ouellet, Y., Dewilde, S., Friedman, J., Ascenzi, P., Guertin, M., and Bolognesi, M. (2004) *J. Biol. Chem.* **279,** 21520–21525
29. Milani, M., Ouellet, Y., Ouellet, H., Guertin, M., Boffi, A., Antonini, G., Bocedi, A., Mattu, M., Bolognesi, M., and Ascenzi, P. (2004) *Biochemistry* **43,** 5213–5221
30. Bolognesi, M., Rosano, C., Losso, R., Borassi, A., Rizzi, M., Wittenberg, J. B., Boffi, A., and Ascenzi, P. (1999) *Biophys. J.* **77,** 1093–1099
31. Bolognesi, M., Cannillo, E., Ascenzi, P., Giacometti, G. M., Merli, A., and Brunori, M. (1982) *J. Mol. Biol.* **158,** 305–315
32. Perutz, M. F. (1989) *Trends Biochem. Sci.* **14,** 42–44
33. Kraulis P. J. (1991) *J. Appl. Crystallogr.* **24,** 946–950
34. Merritt, E. A., and Murphy, M. E. (1994) *Acta Crystallogr. D Biol. Crystallogr.* **50,** 869–873

Structural Determinants in the Group III Truncated Hemoglobin from *Campylobacter jejuni*

Marco Nardini, Alessandra Pesce, Marie Labarre, Christian Richard, Alessandro Bolli, Paolo Ascenzi, Michel Guertin and Martino Bolognesi

J. Biol. Chem. 2006, 281:37803-37812.
doi: 10.1074/jbc.M607254200 originally published online October 5, 2006
